Three-Dimensional van Hove Singularities and Charge Density Wave Evolution in Kagome Lattice KV_3Sb_5

Yu Huang[1,2,3†], Haiyang Ma[4†], Wei Xia[5,6,7†], Zhicheng Jiang[8†], Wenchuan Jing[1], Xiangqi Liu[5], Jiayu Liu[1], Yuming Shi[1], Xun Ma[8], Runfeng Zhang[8], Jin-Feng Jia[9], Jishan Liu[2,10], Mao Ye[2,10], Zhengtai Liu[2,10*], Yanfeng Guo[5,6,7*], and Dawei Shen[8*]

[1]*Shanghai Institute of Microsystem and Information Technology, Chinese Academy of Sciences, Shanghai 200050, China*
[2]*Shanghai Synchrotron Radiation Facility, Shanghai Advanced Research Institute, Chinese Academy of Sciences, Shanghai 201210, China*
[3]*University of Chinese Academy of Sciences, Beijing 100049, China*
[4]*Quantum Science Center of Guangdong-Hong Kong-Macao Greater Bay Area, Shenzhen 518045, China*
[5]*School of Physical Science and Technology, ShanghaiTech University, Shanghai 201210, China*
[6]*ShanghaiTech Laboratory for Topological Physics, ShanghaiTech University, Shanghai 201210, China*
[7]*State Key Laboratory of Quantum Functional Materials, School of Physical Science and Technology, ShanghaiTech University, Shanghai 201210, China*
[8]*National Synchrotron Radiation Laboratory, University of Science and Technology of China, Hefei 230029, China*
[9]*Key Laboratory of Artificial Structures and Quantum Control (Ministry of Education), TD Lee Institute, School of Physics and Astronomy, Shanghai Jiao Tong University, Shanghai 200240, China*
[10]*National Key Laboratory of Materials for Integrated Circuits, Shanghai Institute of Microsystem and Information Technology, Chinese Academy of Sciences, Shanghai 200050, China*

(Received 21 August 2025; accepted manuscript online 16 October 2025)

The kagome metals AV_3Sb_5 (A = K, Rb, Cs) feature intertwined Dirac fermions, topological flat bands, and van Hove singularities (vHS) near the Fermi level, which give rise to a range of exotic, strongly correlated phenomena such as charge density waves (CDW) and superconductivity. Although the vHS from V 3d states have been implicated in CDW formation, their three-dimensional nature and temperature evolution remain poorly understood. In this study, we used high-resolution angle-resolved photoemission spectroscopy and density functional theory to reveal pronounced out-of-plane dispersion of vHS and their temperature dependence in KV_3Sb_5. The identified c-axis band folding and scattering channels were directly linked to the CDW order. These results demonstrate that the CDW transition in this family involves cooperative coupling between electron correlations and structural modulation along the c axis. This offers new insights into the interplay of topology, correlations, and lattice instabilities in kagome metals.

DOI: 10.1088/0256-307X/42/12/120704 CSTR: 32039.14.0256-307X.42.12.120704

Kagome lattice materials, characterized by inherent geometric frustration and exotic electronic band structures, have emerged as model systems for investigating novel quantum phenomena.[1–10] Within this class, the AV_3Sb_5 (A = K, Rb, Cs) family has attracted particular interest because of the simultaneous presence of van Hove singularities (vHS),[11–13] Dirac fermions,[14–16] and topologically nontrivial flat bands[16–20] near the Fermi level (E_F). This unique band structure provides fertile ground for realizing correlated electronic phases, most notably charge-density waves (CDW)[21–26] and superconductivity.[27–31] In particular, the CDW state, manifesting various symmetry-breaking events in AV_3Sb_5, has been intensively studied for its possible role in generating exotic phenomena that include time-reversal symmetry breaking,[21,32–35] orbital loop currents,[36–38] and unconventional superconductivity.[16,30,39,40]

Despite extensive research, the microscopic mechanism underlying CDW formation in AV_3Sb_5 remains highly controversial and is actively debated. Early proposals invoked a primary electronic mechanism driven by nesting between the in-plane vHS.[12,41] However, mounting evidence on lattice distortions and phonon softening[42,43] suggests that lattice degrees of freedom also play a significant role, leading to the prevailing picture of a cooperative electron-lattice mechanism dominated by in-plane interactions.[24,44] More recently, experimental evidence from scanning tunnel-

†These authors contributed equally to this work.
*Corresponding authors. Email: liuzt@sari.ac.cn; guoyf@shanghaitech.edu.cn; dwshen@ustc.edu.cn
© 2025 Chinese Physical Society and IOP Publishing Ltd. All rights, including for text and data mining, AI training, and similar technologies, are reserved.

ing microscopy/spectroscopy (STM/STS),[39,45,46] angle-resolved photoemission spectroscopy (ARPES),[47] and magnetoresistance measurements[46,48–50] have revealed the emergence of a C_2-symmetric electronic ground state below the CDW transition temperature ($T_{\rm CDW}$), suggesting intrinsic electronic nematicity accompanied by the emergence of a three-dimensional (3D) CDW component in AV_3Sb_5.[50–52] Interlayer coupling is increasingly being recognized as crucial for stabilizing the 3D CDW order in AV_3Sb_5.[47,53,54] Specifically, recent studies have demonstrated that distinct CDW stacking configurations (e.g., a π-shift inverted star of David (π-ISD)[55,56]) can significantly lower the energy levels of the vHS, whereas electron-electron interactions favor a $2 \times 2 \times 2$ CDW ground state.[45,56–58] Furthermore, ultrafast time-resolved ARPES experiments on KV_3Sb_5 have revealed cooperative interactions between electronic correlations and lattice distortions during the formation of the 3D CDW state.[59] Although the vHS associated with V 3d electrons have been widely regarded as a key driver of the CDW instability in this class of compounds, crucial spectroscopic details remain unresolved. In particular, the influence of the out-of-plane (k_z) dispersion of vHS and its role in shaping CDW-induced energy gaps remain undetermined. Resolving these 3D electronic characteristics is essential for a comprehensive understanding of the microscopic mechanisms governing CDW formation in AV_3Sb_5.

In this study, we focus on KV_3Sb_5, whose pronounced 3D CDW character and favorable spectroscopic accessibility enable a systematic investigation of the vHS, using temperature- and photon-energy-dependent ARPES[60] complemented by density functional theory (DFT) calculations. Our experimental results revealed a pronounced k_z dispersion of the vHS and distinct out-of-plane band folding in the CDW state, accompanied by an additional electron scattering channel along the c axis. Notably, the evolution of the out-of-plane folding closely tracks the CDW order parameter, providing direct evidence of a cooperative mechanism between electronic correlations and structural dynamics. These results fill a critical gap in the understanding of KV_3Sb_5 and offer broader insights into the intricate interplay among electronic correlations, dimensionality, and quantum order in kagome metals and related correlated systems.[5,24,39,40,45,46]

Single-crystal KV_3Sb_5 crystallizes in a layered hexagonal structure with space group $P6/mmm$ (No. 191), as illustrated in Fig. 1(a). This structure features V atoms forming kagome layers stacked along the c-axis. High-resolution X-ray diffraction measurements [Fig. 1(b)] confirm the excellent crystalline quality of the samples, yielding refined lattice parameters: $a = b = 5.4823$ Å, $c = 8.9493$ Å, with $\alpha = \beta = 90°$ and $\gamma = 120°$, constrained by symmetry. Core-level photoemission spectroscopy performed on the cleaved surfaces reveals sharp peaks corresponding to the Sb 4d and V 3p orbitals [Fig. 1(c)], providing clear elemental identification and confirming surface integrity. The temperature-dependent resistivity [Fig. 1(d)] displays a pronounced anomaly near 78 K, corresponding to $T_{\rm CDW}$ and aligns with prior reports.[14,15,39]

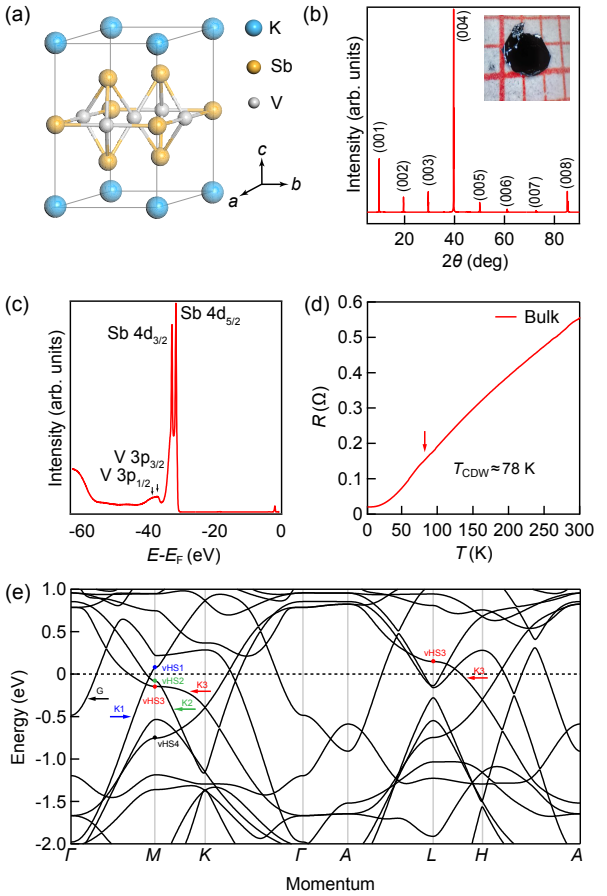

Fig. 1. Basic properties and DFT calculations for KV_3Sb_5. (a) Crystal structure of KV_3Sb_5 (K, V, and Sb atoms are shown as blue, gray, and gold spheres, respectively). (b) Single-crystal X-ray diffraction pattern along the (001) direction (inset: optical image of a single crystal). (c) Core-level photoemission spectrum measured using 88 eV photons, showing V 3p and Sb 4d peaks. (d) Temperature-dependent electrical resistivity. (e) DFT-calculated band structure without spin-orbit coupling (SOC).

The bulk electronic band structure calculated using DFT is shown in Fig. 1(e) and reveals several key features characteristic of kagome metals, including multiple vHS near the M point of the Brillouin zone (BZ). In particular, vHS1, which arises from the K1 band, lies above the Fermi level ($E_{\rm F}$), whereas vHS2 and vHS3, which originate from the K2 and K3 bands, respectively, are located below $E_{\rm F}$. These V 3d kagome-derived vHS play a central role in driving the charge order in KV_3Sb_5 and have been experimentally validated by prior ARPES studies.[10,47,61,62] Detailed examination of the DFT band structure reveals that the bands hosting vHS exhibit significant out-of-plane dispersion, as shown in Fig. 1(e). This 3D characteristic of vHS bands offers crucial insight into the interplay between the 3D CDW order and kagome lattice-derived electronic states near $E_{\rm F}$.

To acquire deeper insight into the key band structure characteristics in the vicinity of $E_{\rm F}$ and the evolution of 3D electronic states in the layered kagome compound KV_3Sb_5, photon-energy-dependent ARPES measurements were performed systematically. Our primary experimental

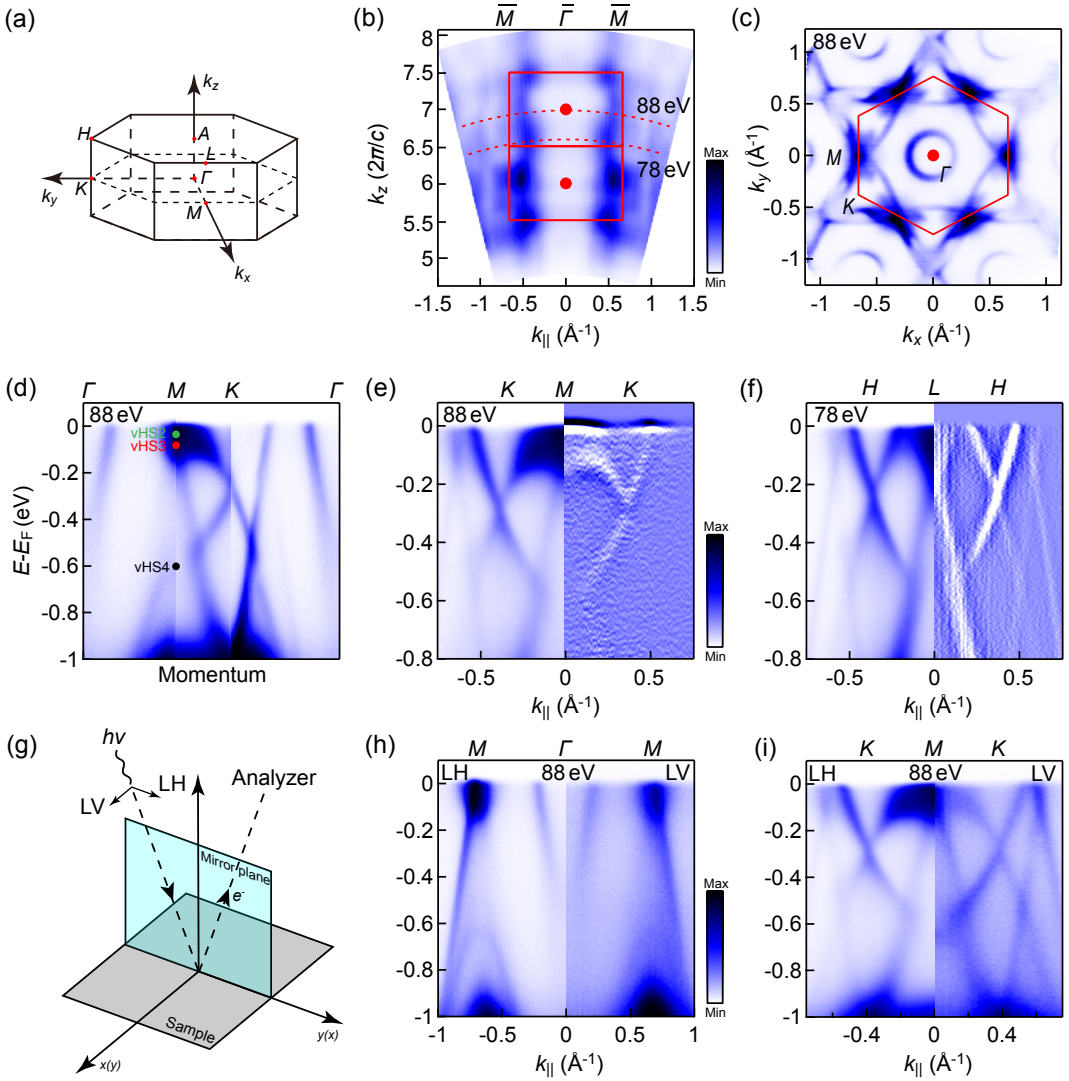

Fig. 2. Constant-energy surface mapping and ARPES intensity plots of KV_3Sb_5 along high-symmetry paths. (a) Schematic of 3D Brillouin zone of KV_3Sb_5. (b) Constant energy surface in the k_z-$k_{\parallel}$ plane at $E_B = 1.2$ eV, where the dashed lines correspond to photon energies of 78 eV and 88 eV, respectively. (c) Fermi surface mapping at $T = 6$ K. (d) Band dispersions along high-symmetry directions showing three vHS located at point M below E_F. (e) and (f) Band dispersion along the K–M–K/H–L–H direction: the left panels show raw spectra, and the right panels show energy- and momentum-second-derivative spectra, respectively. (g) Schematic of the experimental geometry used for polarization-dependent ARPES. (h) and (i) Polarization-resolved ARPES spectra along the Γ–M and K–M directions, with the left and right halves corresponding to LH and LV polarization, respectively.

strategy was to precisely locate the momentum positions of the relevant electronic bands within the 3D BZ, as shown in Fig. 2(b). We acquired spectral intensity maps across the $k_{\parallel} - k_z$ plane within the photon energy ($h\nu$) range of 40 $\sim$ 120 eV, where k_z is the out-of-plane component of the momentum vector. At a binding energy (E_B) of 1.2 eV, we observed clear periodic intensity modulations along k_z at the M point, which are also reproduced at other binding energies [see Figs. S1 and S2 of Supplementary Materials (SM) for details], indicative of significant out-of-plane dispersion of the associated bands. By fitting the k_z-dependent dispersion, we determined the inner potential of $V_0 \approx 8$ eV, to establish the photon energies $h\nu \approx 88$ eV and $h\nu \approx 78$ eV that should be used to probe the $k_z = 0$ and $k_z = \pi$ planes, respectively. The orbital-projected DFT calculations (Fig. S3 in SM) reveal that the bands exhibiting strong k_z dependence near the M point predominantly originate from the V 3d orbitals. These orbitals generate two van Hove singularities (vHS2 and vHS3) located close to E_F.

Next, to resolve the detailed band dispersion near E_F, high-resolution ARPES scans were acquired along the high-symmetry path Γ–M–K–Γ at $k_z = 0$ ($h\nu \approx 88$ eV) to successfully capture multiple vHS features [Fig. 2(d)]. The DFT calculations show that vHS1 and vHS2, both located at the M point, vanish in the $k_z = \pi$-plane, whereas vHS3 shifts to approximately 200 meV above E_F [Fig. 1(e)]. This k_z-dependent evolution of the vHS features leads to a significantly reduced density of states near E_F at the L point (equivalent to the M point at $k_z = \pi$) compared with the M point at $k_z = 0$. This observation directly explains the strong spectral weight contrast between the M and L points in our photon-energy-dependent ARPES measurements [Figs. 2(e) and 2(f)].

Motivated by these observations, we used polarization-dependent ARPES to disentangle the orbital origins of vHS near E_F. Leveraging photoemission dipole selection rules,[63,64] we employed linearly horizontal (LH) and linearly vertical (LV) polarized light to selectively probe orbital symmetries [Fig. 2(g)]. Polarization-resolved ARPES spectra were acquired along the M–Γ–M and K–M–K directions [Figs. 2(h) and 2(i), respectively]. At the M point, the photoemission intensity under LV polarization exhibits systematic and substantial suppression compared with the LH-polarized case, particularly along the K–M–K direction [Fig. 2(i)]. This pronounced polarization dependence allowed us to assign orbital characteristics to the vHS features through a combined analysis of dipole selection rules and DFT-based orbital-projected calculations (Fig. S3 of SM). Specifically, vHS2 originates primarily from the d_{yz} orbital; vHS3 exhibits a mixed $d_{x^2-y^2}/d_{z^2}$ character; and vHS4 is derived from the $d_{x^2-y^2}/d_{xy}$ orbitals (a detailed analysis is provided in SM). Moreover, orbital-projected electronic state analysis reveals that the vHS3 contributions are predominantly from the d_{z^2} orbital. The substantial out-of-plane character of this orbital accounts for the pronounced k_z-dispersion observed in the corresponding band near the M point. This insight not only confirms the 3D nature of the vHS features but also highlights the key role of orbital-selective dispersion in the electronic structure of KV_3Sb_5.

Van Hove singularities near M play a pivotal role in the formation and stability of CDW order in kagome materials.[12,41,65] To investigate how these vHS evolve across different k_z planes as a function of temperature, we performed systematic temperature-dependent ARPES measurements along the high-symmetry directions K–M–K and L–H–L in momentum space. Our experimental results reveal a direct correlation between the onset of CDW order and reconstruction of the band structure near the M point. In the normal metallic phase [$T > T_{CDW}$, Fig. 3(a)],

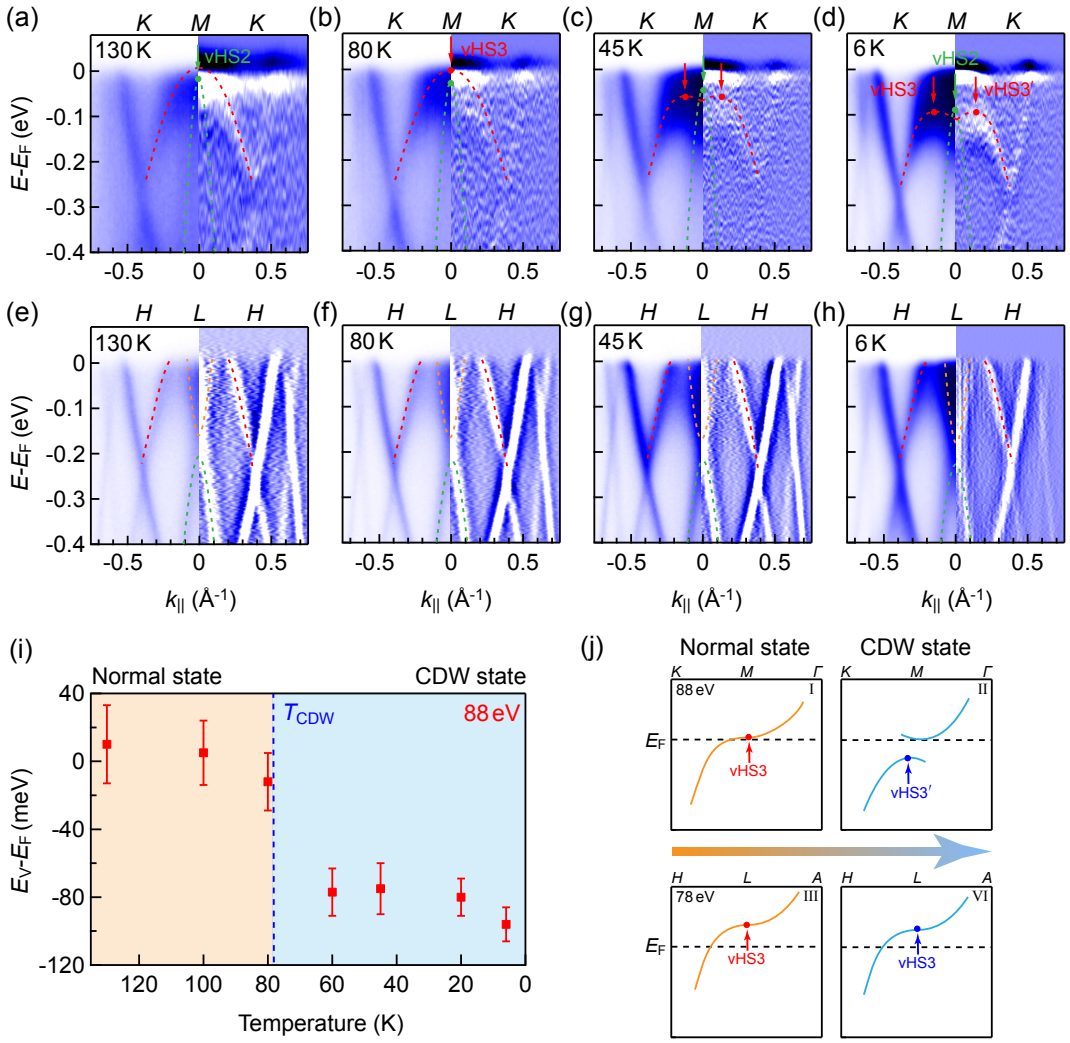

Fig. 3. The temperature dependence of vHS in KV_3Sb_5. (a)–(h) Temperature dependence of the electronic states along the K–M–K/H–L–H direction measured at $h\nu = 88$ eV/78 eV. Dashed curves serve as guides in tracing key bands. (i) Temperature-dependent energy gap between E_F and (E_V) measured at 88 eV. The position of E_V was determined by numerically fitting Lorentzian peaks and convolving with a Fermi-Dirac distribution, using a Shirley background (Fig. S5 of SM). The error bars indicate the uncertainty in determining the magnitude of the energy gap. (j) Schematic illustration of the temperature evolution of the K3 band in different k_z planes.

vHS2 resides just below E_F, whereas vHS3 lies above E_F in the unoccupied states. Upon cooling to the CDW phase [$T < T_{CDW}$, Figs. 3(c) and 3(d)], both features shift toward higher binding energies, with vHS3 exhibiting a notably larger downward shift than vHS2. This band reconstruction results in a characteristic saddle-point configuration at the M point, producing a pronounced M-shaped dispersion accompanied by the emergence of a new singularity, vHS3′, as shown in Fig. S4 of SM. The appearance of vHS3′ significantly enhances the local density of states near E_F, which may facilitate Fermi surface nesting and promote emergent correlated electronic phases, such as superconductivity at lower temperatures.[66,67]

Furthermore, through an analysis of the energy distribution curve (EDC) of our ARPES data, we quantitatively extracted the energy gap between E_F and E_V, which is defined as the binding energy of vHS3′ in the CDW state, as shown in Fig. 3(i). This analysis provides direct evidence of band reconstruction associated with the CDW transition (see Fig. S5 of SM for details). In contrast, the K3 band near the L point shows minor CDW-induced modifications beyond a slight spectral weight redistribution, without any discernible vHS below E_F [Figs. 3(e)–3(h)]. The temperature-dependent evolution of the K3 band at both the M and L points is summarized in Fig. 3(j), highlighting the pronounced downward shift and emergent M-shaped dispersion exclusive to the M point.

However, given the experimentally confirmed presence of interlayer coupling in KV_3Sb_5,[47,54,59] the microscopic mechanism underlying the out-of-plane charge ordering and associated band reconstruction should be elucidated to fully understand the intrinsic $2 \times 2 \times 2$ 3D CDW order of the material. While prior ARPES studies have reported in-plane 2×2 distortion-induced band folding,[47,61] the nature of k_z-dependent electronic reconstruction remains less explored. Figures 4(a)–4(d) present the low-temperature band dispersions and corresponding EDC along the high-symmetry directions K–M–K and H–L–H. Along the K–M direction in the $k_z = 0$ plane, we observe distinct M-shaped hole-like bands, indicative of CDW-induced band reconstruction. In contrast, along the H–L–H path in the $k_z = \pi$ plane, a shallow electron-like band emerges at the L point with a binding energy of approximately 120 meV. The pronounced contrast between the M and L points highlights the momentum-selective and 3D nature of CDW-induced band modifications.

Notably, an additional shoulder-like feature with a binding energy of approximately 100 meV emerges in EDC near the L point, as shown in Fig. 4(d) (see Fig. S6 of SM for details). This feature suggests possible band reconstruction associated with the CDW phase transition. The shoulder-shaped band exhibits a high density of states and the E_B of this matches that of vHS3′ (M-shaped band) near the M point in the CDW phase. This energy alignment strongly supports a scenario in which the vHS3′ at the M point undergoes out-of-plane reconstruction and

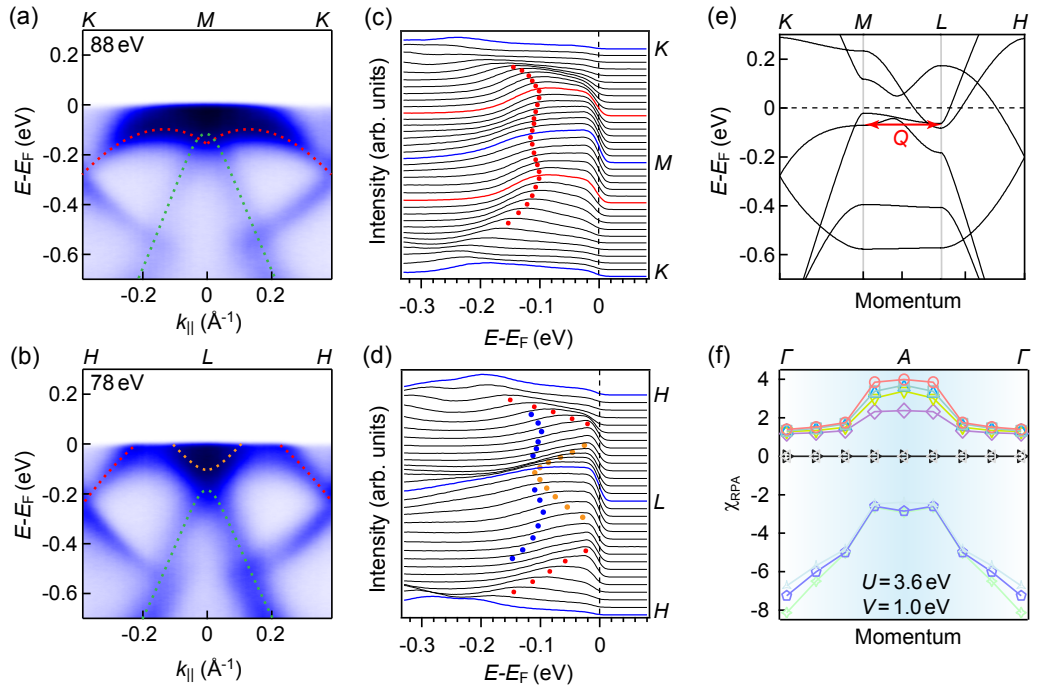

Fig. 4. The interlayer band folding and scattering in KV_3Sb_5. (a) and (b) Energy-momentum (E–k) dispersion along the K–M–K/H–L–H high-symmetry direction measured at 6 K. Dashed curves serve as guides in tracing the key bands. (c) and (d) EDC stacking plots of panels (a) and (b), respectively, with round markers indicating the fitted peak positions (see Method in Fig. S5 of SM). Red: M-point K3 hole pocket; orange: L-point electron pocket; blue: fitted hump position. (e) DFT-calculated band structure of KV_3Sb_5 in K–M–L–H-direction. E_F has shifted downward by 50 meV and the renormalization factor was set to $Z = 0.8$. The scattering vector between points M and L is indicated by a red arrow. (f) Eigenvalues of the generalized RPA susceptibility tensor, plotted along the Γ–A direction and symmetrized about the A point. On-site ($U = 3.6$ eV) and nearest-neighbor Sb–V intersite ($V = 1.0$ eV) interaction parameters were used.

becomes folded to the L point through 3D BZ folding. This provides direct experimental evidence for the out-of-plane band reconstruction in the 3D CDW state.

Further insights are provided by the DFT calculations shown in Fig. 4(e), which depict the band evolution along the M–L direction. Two electron pockets are predicted near the L point, originating from the hybridization of the V (d_{yz}/d_{xz}) and Sb (p_z) orbitals. As shown in the orbitally resolved projections (Fig. S3 of SM), the bottom of these electron pockets aligns well in energy with the V d_{z^2}-dominated vHS3′ band near the M point. This energy matching, combined with the presence of interlayer orbital hybridization and synergistic role of the V–Sb sublattice environment, suggests that the momentum connection between the M-shaped hole-like band at the M point and electron pockets at the L point (with matched k_z components) may constitute a key interlayer scattering channel. This channel may be essential for enabling out-of-plane Fermi surface nesting in the 3D CDW phase. [23,68,69]

To further elucidate the nature of the out-of-plane electronic structure modulation in the 3D CDW state, we performed random phase approximation (RPA) susceptibility χ_{RPA} calculations to estimate the potential charge and spin density of wave instabilities. KV_3Sb_5 undergoes a $2\times2\times2$ π-ISD type CDW transition at $T_{\mathrm{CDW}} \approx 78$ K, with the corresponding structural modulation shown in Fig. S7 of SM. To probe the collective response of the system, we computed the eigenmodes of the RPA polarizability tensor along the Γ–A direction, following the method described in Ref. [70]. As shown in Fig. 4(f), the ten largest eigenmodes of the response function exhibit a sharp peak near $\boldsymbol{q} = (0, 0, 0.5)$, namely the zone-boundary A point in reciprocal space. This dominant response wavevector corresponds precisely to the k_z component ($0.5 \times 2\pi/c$) of the M–L scattering channel identified experimentally, providing strong evidence for a momentum-selective k_z-matching scattering mechanism that stabilizes the out-of-plane CDW order at the susceptibility level. In addition, phonon spectrum calculations revealed pronounced softening at both the M and L points in the BZ of AV_3Sb_5, corroborating that phonon instabilities also play a critical role in CDW formation. [24,42,47] These findings collectively establish that the synergistic interplay between interlayer electronic correlations and lattice phonon coupling constitutes the core microscopic mechanism driving the emergence of the long-range 3D $2 \times 2 \times 2$ CDW order in KV_3Sb_5.

In summary, we elucidated the temperature-dependent evolution of 3D vHS in the kagome metal KV_3Sb_5, which was determined through high-resolution ARPES measurements and corroborated by DFT calculations. Our results reveal pronounced out-of-plane dispersion in the vHS-derived bands, along with distinct band folding that emerges below the CDW transition temperature. RPA susceptibility calculations further demonstrate that the M–L interlayer electron scattering channel not only drives the observed band folding but also highlights a cooperative mechanism between electronic correlations and lattice structural dynamics. These findings provide fundamental insights into the microscopic origin of the 3D CDW order and advance our understanding of electron-phonon coupling in geometrically frustrated quantum materials.

Acknowledgments. We thank the Shanghai Synchrotron Radiation Facility (SSRF) of BL03U (31124.02.SSRF.BL03U) for their assistance with ARPES measurements. This work was supported by the National Key R&D Program of China (Grant Nos. 2023YFA1406304 and 2024YFA1408103), the National Science Foundation of China (Grant Nos. 12494593 and 12004405), and the Anhui Provincial Natural Science Foundation (Grant No. 2408085J003). Y. F. Guo acknowledges the National Key R&D Program of China (Grant No. 2023YFA1406100) and the open projects of the State Key Laboratory of Functional Materials for Informatics (Grant No. SKL2022), CAS. Z. C. Jiang acknowledges the China National Postdoctoral Program for Innovative Talents (BX20240348). W.X. acknowledges support from the National Natural Science Foundation of China (Grant No. 12404186) and the Shanghai Sailing Program (Grant No. 23YF1426900).

References

[1] Guo H M and Franz M 2009 *Phys. Rev. B* **80** 113102
[2] O'Brien A, Pollmann F, and Fulde P 2010 *Phys. Rev. B* **81** 235115
[3] Nakatsuji S, Kiyohara N, and Higo T 2015 *Nature* **527** 212
[4] Norman M R 2016 *Rev. Mod. Phys.* **88** 041002
[5] Yin J X, Zhang S S, Li H *et al.* 2018 *Nature* **562** 91
[6] Ye L, Kang M G, Liu J W *et al.* 2018 *Nature* **555** 638
[7] Liu E K, Sun Y, Kumar N *et al.* 2018 *Nat. Phys.* **14** 1125
[8] Yin J X, Zhang S S, Chang G Q *et al.* 2019 *Nat. Phys.* **15** 443
[9] Liu D F, Liang A J, Liu E K *et al.* 2019 *Science* **365** 1282
[10] Yang S Y, Wang Y J, Ortiz B R *et al.* 2020 *Sci. Adv.* **6** 6003
[11] Kiesel M L, Platt C, and Thomale R *et al.* 2013 *Phys. Rev. Lett.* **110** 126405
[12] Cho S, Ma H Y, Xia W *et al.* 2021 *Phys. Rev. Lett.* **127** 236401
[13] Scammell H D, Ingham J L, Li T, and Sushkov O P2023 *Nat. Commun.* **14** 605
[14] Ortiz B R, Gomes L C, Morey J R *et al.* 2019 *Phys. Rev. Mater.* **3** 094407
[15] Ortiz B R, Sarte P M, Kenney E M *et al.* 2021 *Phys. Rev. Mater.* **5** 034801
[16] Ortiz B R, Teicher S M L, Hu Y *et al.* 2020 *Phys. Rev. Lett.* **125** 247002
[17] Hu Y, Teicher S M L, Ortiz B R *et al.* 2022 *Sci. Bull.* **67** 495
[18] Jiang Z C, Liu Z T, Ma H Y *et al.* 2023 *Nat. Commun.* **14** 4892
[19] Wang Y, Liu Y X, Hao Z Y *et al.* 2023 *Chin. Phys. Lett.* **40** 037102
[20] Jing W C, Liu Z T, Jiang Z C *et al.* 2025 *Phys. Rev. B* **111** 205134
[21] Lin Y P and Nandkishore R M 2021 *Phys. Rev. B* **104** 045122
[22] Park T, Ye M X, and Balents L 2021 *Phys. Rev. B* **104** 035142
[23] Li H X, Zhang T T, Yilmaz T *et al.* 2021 *Phys. Rev. X* **11** 031050
[24] Tan H X, Liu Y Z, Wang Z Q, and Yan B H 2021 *Phys. Rev. Lett.* **127** 046401

[25] Christensen M H, Birol T, Andersen B M, and Fernandes R M 2021 *Phys. Rev. B* **104** 214513
[26] Ortiz B R, Teicher S M L, Kautzsch L 2021 *Phys. Rev. X* **11** 041030
[27] Wu X X, Schwemmer T, Müller T *et al.* 2021 *Phys. Rev. Lett.* **127** 177001
[28] Chen K Y, Wang N N, Yin Q W *et al.* 2021 *Phys. Rev. Lett.* **126** 247001
[29] Xu H S, Yan Y J, Yin R T *et al.* 2021 *Phys. Rev. Lett.* **127** 187004
[30] Yin Q W, Tu Z J, Gong C S *et al.* 2021 *Chin. Phys. Lett.* **38** 037403
[31] Neupert T, Michael Denner M, Yin J X, Thomale R, and Zahid Hasan M 2022 *Nat. Phys.* **18** 137
[32] Mielke III C, Das D, Yin J X *et al.* 2022 *Nature* **602** 245
[33] Khasanov R, Das D, Gupta R *et al.* 2022 *Phys. Rev. Res.* **4** 023244
[34] Zhang W, Liu X Y, Wang L F *et al.* 2023 *Nano Lett.* **23** 872
[35] Deng H, Liu G W, Guguchia Z *et al.* 2024 *Nat. Mater.* **23** 1639
[36] Christensen M H, Birol T, Andersen B M, and Fernandes R M 2022 *Phys. Rev. B* **106** 144504
[37] Zhou S and Wang Z Q 2022 *Nat. Commun.* **13** 7288
[38] Li Q F, Pan G P, Zhang X *et al.* 2025 *Chin. Phys. Lett.* **42** 057302
[39] Jiang Y X, Yin J X, Michael Denner M *et al.* 2021 *Nat. Mater.* **20** 1353
[40] Jiang K, Wu T, Yin J X *et al.* 2023 *Natl. Sci. Rev.* **10** 199
[41] Kang M G, Fang S, Kim J K *et al.* 2022 *Nat. Phys.* **18** 301
[42] Uykur E, Ortiz B R, Wilson S D, Dressel M, and Tsirlin A A 2022 *npj Quantum Mater.* **7** 16
[43] Subedi A 2022 *Phys. Rev. Mater.* **6** 015001
[44] Xie Y F, Chalus N, Wang Z W *et al.* 2024 *Nat. Commun.* **15** 6467
[45] Liang Z W, Hou X Y, Zhang F *et al.* 2021 *Phys. Rev. X* **11** 031026
[46] Zhao H, Li H, Ortiz B R *et al.* 2021 *Nature* **599** 216
[47] Jiang Z C, Ma H Y, Xia W *et al.* 2023 *Nano Lett.* **23** 5625
[48] Xiang Y, Li Q, Li Y K *et al.* 2021 *Nat. Commun.* **12** 6727
[49] Ni S L, Ma S, Zhang Y H *et al.* 2021 *Chin. Phys. Lett.* **38** 057403
[50] Li H, Zhao H, Ortiz B R *et al.* 2022 *Nat. Phys.* **18** 265
[51] Denner M M, Thomale R, and Neupert T 2021 *Phys. Rev. Lett.* **127** 217601
[52] Nie L P, Sun K L, Ma W R *et al.* 2022 *Nature* **604** 59
[53] Watkins A K, Johrendt D, Vlcek V, Wilson S D, and Seshadri R 2024 *Phys. Rev. Mater.* **8** 054204
[54] Dong J W, Lin Y H, Fu R Q, Su G, Wang Z Q, and Zhou S 2025 *Phys. Rev. B* **111** 045155
[55] Li H Q, Liu X Y, Kim Y B, and Kee H Y 2023 *Phys. Rev. B* **108** 075102
[56] Kang M G, Fang S, Yoo J *et al.* 2023 *Nat. Mater.* **22** 186
[57] Hu Y, Wu X X, Ortiz B R *et al.* 2022 *Phys. Rev. B* **106** L241106
[58] Zhu H E, Li T R, Yu F H *et al.* 2023 *Chin. Phys. Lett.* **40** 047301
[59] Liu H R, Duan S F, Liu X Q *et al.* 2025 *Sci. Bull.* **70** 1211
[60] Yang Y C, Liu Z T, Liu J S *et al.* 2021 *Nucl. Sci. Tech.* **32** 31
[61] Luo H L, Gao Q, Liu H X *et al.* 2022 *Nat. Commun.* **13** 273
[62] Kato T, Li Y K, Kawakami T *et al.* 2022 *Commun. Mater.* **3** 30
[63] Damascelli A, Hussain Z, and Shen Z X 2003 *Rev. Mod. Phys.* **75** 473
[64] Hu Y, Wu X X, Ortiz B R *et al.* 2022 *Nat. Commun.* **13** 2220
[65] Zhou X X, Li Y K, Fan X W *et al.* 2021 *Phys. Rev. B* **104** L041101
[66] Terashima K, Sekiba Y, Bowen J H, and Takahashi T 2009 *Proc. Natl. Acad. Sci.* **106** 7330
[67] Deng J Z, Zhang R H, Xie Y, Wu X X, and Wang Z J 2023 *Phys. Rev. B* **108** 115123
[68] Kiesel M L and Thomale R 2012 *Phys. Rev. B* **86** 121105
[69] Ritz E T, Røising H S, Christensen M H, Birol T, Andersen B M, and Fernandes R M 2023 *Phys. Rev. B* **108** L100510
[70] Ma H Y, Yin J X, Zahid Hasan M, and Liu J P 2022 *Phys. Rev. B* **106** 155125